PHYSICAL REVIEW C **80**, 034316 (2009)

Breakup channels for ^{12}C triple-α continuum states

C. Aa. Diget,[1,2,*] F. C. Barker,[3] M. J. G. Borge,[4] R. Boutami,[4] P. Dendooven,[5] T. Eronen,[6] S. P. Fox,[1] B. R. Fulton,[1]
H. O. U. Fynbo,[2] J. Huikari,[7] S. Hyldegaard,[2] H. B. Jeppesen,[2] A. Jokinen,[6] B. Jonson,[8] A. Kankainen,[6]
I. Moore,[6] A. Nieminen,[6] G. Nyman,[8] H. Penttilä,[6] V. F. E. Pucknell,[9] K. Riisager,[2] S. Rinta-Antila,[6]
O. Tengblad,[4] Y. Wang,[6] K. Wilhelmsen,[8] and J. Äystö[6]
[1]*Department of Physics, University of York, York, YO10 5DD, United Kingdom*
[2]*Department of Physics and Astronomy, University of Aarhus, DK-8000 Århus, Denmark*
[3]*Department of Theoretical Physics, Research School of Physical Sciences and Engineering,*
The Australian National University, Canberra ACT 0200, Australia
[4]*Instituto Estructura de la Materia, CSIC, E-28006 Madrid, Spain*
[5]*Kernfysisch Versneller Institut, University of Groningen, Zernikelaan 25, 9747 AA Groningen, The Netherlands*
[6]*Department of Physics, University of Jyväskylä, FIN-40014 Jyväskylä, Finland*
[7]*CEN Bordeaux-Gradignan, Le Haut-Vigneau, F-33175 Gradignan Cedex, France*
[8]*Fundamental Physics, Chalmers University of Technology, S-41296 Göteborg, Sweden*
[9]*CCLRC Daresbury Laboratory, Daresbury Warrington, Cheshire WA4 4AD, United Kingdom*

(Received 9 March 2009; published 22 September 2009)

The triple-α-particle breakup of states in the triple-α continuum of ^{12}C has been investigated by way of coincident detection of all three α particles of the breakup. The states have been fed in the β decay of ^{12}N and ^{12}B, and the α particles measured using a setup that covers all of the triple-α phase space. Contributions from the breakup through the ^{8}Be(0^+) ground state as well as other channels—interpreted as breakup through excited energies in ^{8}Be—have been identified. Spins and parities of ^{12}C triple-α continuum states are deduced from the measured phase-space distributions for breakup through ^{8}Be above the ground state by comparison to a fully symmetrized sequential R-matrix description of the breakup. At around 10 MeV in ^{12}C, the breakup is found to be dominated by 0^+ strength breaking up through the ghost of the ^{8}Be(0^+) ground state with $L = 0$ angular momentum between the first emitted α particle and the intermediate ^{8}Be nucleus. For ^{12}C energies above the 12.7 MeV 1^+ state, however, $L = 2$ breakup of a ^{12}C 2^+ state through the ^{8}Be(2^+) excited state dominates. Furthermore, the possibility of a 2^+ excited state in the 9–12 MeV region of ^{12}C is investigated.

DOI: 10.1103/PhysRevC.80.034316 PACS number(s): 23.40.−s, 26.20.Fj, 27.20.+n

I. INTRODUCTION

Recent technological developments, in particular in the field of radioactive beams, has allowed many aspects of nuclear structure, including the study of cluster structures [1], to be reassessed. One of the open questions that has attracted recent interest is the resonances in ^{12}C with pronounced α-particle structure, in particular the 0^+ and 2^+ states above the Hoyle state. It has become clear that the third 0^+ state (0_3^+) is situated at 10- to 11-MeV excitation energy [2–4] although a consistent picture incorporating all data is still not established. Furthermore, the properties of the second 2^+ state (2_2^+) remain unclear. Recent theoretical calculations indicate that it should lie in the same energy range as the 0_3^+ state; see Refs. [5,6] and references therein. Quite apart from the nuclear physics interest, the exact position of the 2_2^+ may influence the triple-α reaction rate in stars [7–10].

Two factors make the unraveling of the ^{12}C spectrum above the 7.275-MeV triple-α threshold particularly challenging. The first is the broad profiles of some of the ^{12}C resonances that makes it hard to single them out in even the most selective spectra. The second is the very high α-clustering present in all relevant ^{8}Be ("double-α") states, implying that all these states couple strongly to the continuum. This further broadens the features in the experimental spectra and makes it harder to distinguish—both experimentally and conceptually—between sequential and direct breakup mechanisms. The experimental challenge is that with the intermediate ^{8}Be states being broader than the typical α energies, even a strictly sequential breakup through such states may—depending on the spin of the involved states—cover large regions of the triple-α phase space, resembling a direct breakup. Conceptually, the description of the breakup is further complicated as the breakup may not be strictly sequential or direct but lie in between the two extremes. This question arises in general for three-body final states (see Ref. [11] for other recent examples) but is even more challenging here because the three final-state particles are identical.

However, the experiment benefits from several properties of the states and decays involved. First, as the α particles are spin zero particles and furthermore are identical, the number of partial wave combinations allowed in the breakup is very limited. Second, the level density is relatively low for ^{12}C as well as for the intermediate ^{8}Be nucleus in the region of interest. For ^{12}C the density of populated levels is further reduced by the selectivity of the β decay, which from the 1^+ ground states of ^{12}N and ^{12}B populates only the 0^+, 1^+, and 2^+ states of ^{12}C. A complete kinematics experiment therefore

---

[*] cd550@york.ac.uk

allows sufficient information to be extracted to distinguish many features of the decay [12–14], but we note for later use that the distinction between sequential and direct breakup [15] can in some cases be experimentally very subtle [16]. We can therefore employ R-matrix parametrizations as acceptable first approximations of the decay spectra; this will be used in the simulations below.

The present article reports on a complete kinematics experiment with coincident detection of the three α particles emitted following the β decay of ^{12}B and ^{12}N; a more complete account can be found in Ref. [17]. After a description of the experimental setup in Sec. II, the main features of the analysis procedures are given in Sec. III. The following sections report on the main results that can be extracted exclusively from these data, i.e., identification of the decay mechanisms and decay channels and a determination of the spin of the contributing ^{12}C resonances based on the observed energy and angular correlations. The latter analysis relies heavily on Dalitz plots and extensive simulations of the decay. The two main limitations of the present experiment, an energy threshold more than one MeV above the Hoyle state and a detection efficiency that depends on the decay pattern, can be overcome in total absorption experiments where the total triple-α energy is measured directly. However, these suffer from lack of knowledge of the decay sequence. The optimal strategy is to combine the two approaches to obtain a more consistent picture of the decay and part of the present data therefore has been combined with data from a total absorption experiment. Separate publications report these results: An analysis of the absolute branching ratios can be found in Refs. [18,19] and an R-matrix fit of the total data sets is in progress. We shall refrain from attempting a partial fit of the present data alone, because the Hoyle state that lies below our detection threshold is known [2] to have a substantial effect on the spectra up to several MeV above its nominal position. That seemingly narrow levels can contribute in this way will be shown in the present article to be the case also for the ^{8}Be ground state.

II. EXPERIMENTAL SETUP

As in previous experiments [2,8,12], we have in the present measurement made use of the β decay of ^{12}B and ^{12}N to populate ^{12}C states of spin and parity 0^+, 1^+, and 2^+ exclusively (Fig. 1). This is done to cope with the presence of other states in this energy region [20], many of which were populated in the previous inelastic-scattering experiments [3,4,13,21,22]. The populated resonances above threshold can all decay to three α particles, and the triple-α breakup of these states is measured using a segmented detector setup as shown in Fig. 2, similar to the approach in our previous experiments. The present experiment goes beyond the preceding in several ways; first, by combining detection of β-delayed triple-α breakup from ^{12}B and ^{12}N in a single experiment. The different β-decay Q values imply that the β-decay phase spaces for the two decays each weight the populated ^{12}C states differently, resulting in two complementary ^{12}C energy spectra. Second, in the previous experiments it was possible only to detect triple-α breakup through low energies in ^{8}Be, that is, through

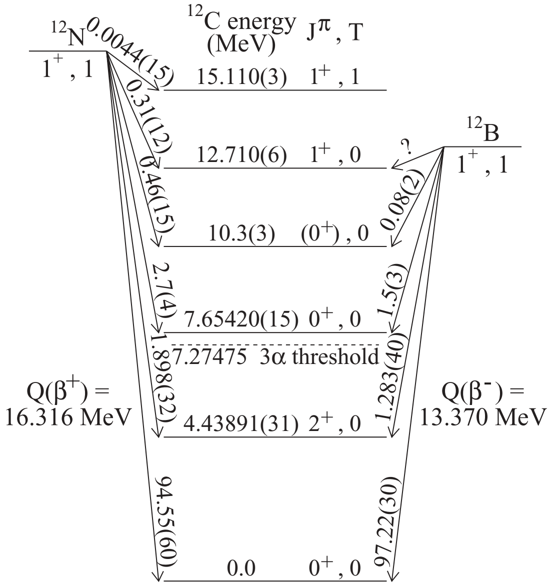

FIG. 1. States in ^{12}C with β-decay feeding according to Ref. [20]. Recently an improved set of branching ratios have been published [18].

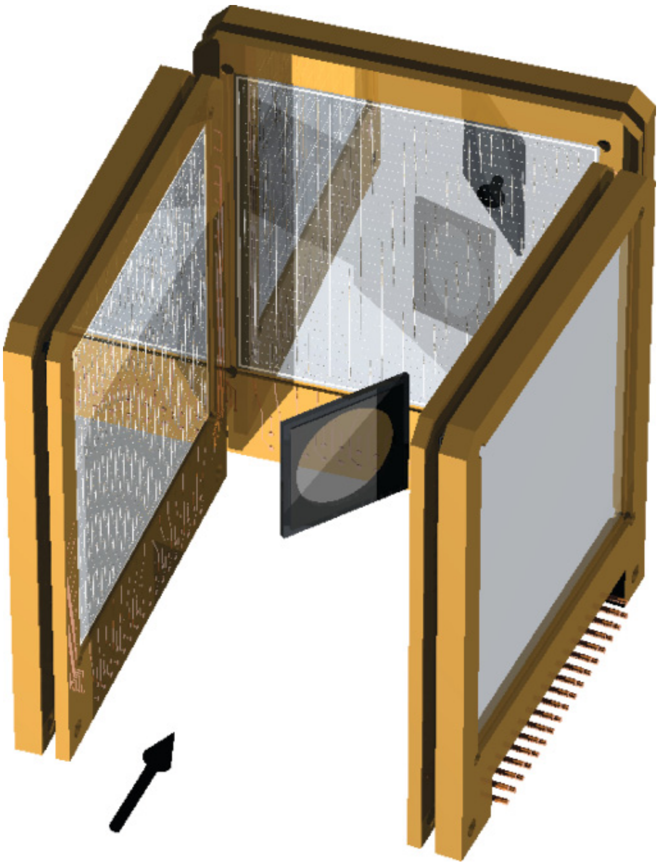

FIG. 2. (Color online) Compact geometry setup: Surrounding a carbon foil are three thin DSSSDs backed by thicker detectors for β detection.

the ^{8}Be ground state 92 keV above the α-α threshold [2]. For non-ground-state energies in ^{8}Be only detection of double-α coincidences was possible [12]. The present experiment is therefore designed to detect breakup of the 0^+ and 2^+ states through excited energies in ^{8}Be. As will become clear in the following, the distinction between ground-state and non-ground-state energies is evident experimentally. However, we cannot at this stage assume that a ^{8}Be excited state plays a role in the breakup, and "excited energies" should therefore be understood only as an observational feature. With the present data we will therefore be able to check the assumption that the ^{8}Be(gs) breakup channel dominates for the 10.3-MeV 0^+ strength and in general investigate the properties of the breakup channels for 0^+ as well as 2^+ states in ^{12}C. Third, the present measurements yield absolute branching ratios for individual states and energy regions in both β decays thereby quantifying the isospin (a-)symmetry in the decays. These results are, however, given elsewhere [18].

The experiment was performed at the IGISOL facility in Jyväskylä, Finland [23], which is the only facility where ISOL beams of both ^{12}N and ^{12}B are presently available. The two isotopes were produced by the ^{12}C$(p,n)^{12}$N and ^{11}B$(d,p)^{12}$B reactions, with a 28-MeV 25-μA proton (10-MeV 10-μA deuteron) beam impinging on a 1400-μg/cm^2 (500-μg/cm^2) target of natural carbon (boron). After mass separation the yield was 300 ions/s (4000 ions/s). With an energy of 25 keV the beams were implanted in a 33-μg/cm^2 carbon foil of 20-mm diameter surrounded by three double-sided silicon strip detectors (DSSSDs) in a compact geometry setup (Fig. 2). With this setup, the three detectors cover the complete three-particle phase space, which yields an increased sensitivity to breakup through excited energies in ^{8}Be. All three detectors are constructed from 50×50 mm^2 Si wafers of thicknesses close to 60 μm, enough to stop the α particles of interest. On the front (back) side they have a thin p-type (n-type) doped layer separated in 16 3.0-mm strips on each side giving a dead layer equivalent to 100 nm silicon. The two detectors facing each other are of a newly developed design [24] where the aluminum contacts are formed as a grid covering only 2% of the active area of the strips to avoid an additional dead layer. However, the DSSSD facing the beam has a total dead layer of 630 nm silicon equivalent because of the contact layer on top of each strip.

All three strip detectors are backed by a 1-mm-thick silicon β detector, in addition to which a germanium γ detector is used for detection of the 4.44-MeV γ from population of the first excited state in ^{12}C. This allows an absolute normalization of the branching ratios to the individual states observed and is discussed in detail elsewhere [18]

A. Calibration

Three different α sources are used in the calibration to ensure that all systematics are under control. A ^{148}Gd source and a ^{241}Am source are used for the actual calibration, while a ^{20}Na source is used for testing the calibration as well as the setup geometry and the dead layer corrections derived from this geometry. These three sources cover the range of α energies from about 2 to 5.5 MeV [25,26]. The ^{20}Na source is produced online using the ^{24}Mg$(p,n\alpha)^{20}$Na reaction at a proton energy of 40 MeV. After separation the ions (approximately 2000 ions/s) are implanted in the carbon foil (Fig. 2) at the same secondary-beam energy as ^{12}N and ^{12}B.

The source positions relative to the detectors are found from the spatial distribution of the α particles hitting the detectors [27]. This is done for the off-line sources as well as for ^{20}Na. For the latter the spatial analysis furthermore determines the position of the detectors relative to the foil, which is needed for the analysis of the ^{12}N and ^{12}B decay data. For the calibration, an effective energy position for each α group as detected by a given pixel is found by calculating the dead layer corrections pixel-by-pixel as done in Ref. [27]. For each strip the effective energy position is then found by weighting the results for each pixel according to the relative intensity in the pixels. For the calibration test as well as for the ^{12}N and ^{12}B data analysis, the energy losses in the foil as well as in the detector dead layer are corrected for on an event-by-event basis. The corrections are in all cases done using the SRIM2003 program package [28].

The ^{20}Na calibration test agrees with the known α lines [26] to within 10–20 keV. The single α energy FWHM resolution is 70 keV. No systematic energy dependence in resolution is seen in any of the strips included in the analysis. The measured relative branching ratios of the eight α groups used are consistent with those given by Ref. [26] but have fewer statistics.

III. ^{12}N AND ^{12}B DECAY DATA

To discriminate between α-particle hits and low-energy background in the form of either electronic noise or β response, a low-energy threshold higher than the data acquisition threshold is introduced in the data analysis. The threshold is set individually for each strip according to the noise levels in that particular strip and is in general lower for the ^{12}B data than for ^{12}N. These cutoffs are chosen so low that for the lowest energies more than 90% of the accepted signals are background. This is done to maximize the acceptance of the cutoff and is reasonable because additional background suppression is introduced subsequently. As for the low-energy cutoffs the trigger levels are lower for the ^{12}B data than for the ^{12}N data.

Typically more than one strip is hit by an α particle, and the front-back energy difference is used to identify matching front-back pairs, thereby determining the position of each hit. For such a hit a maximal energy difference of 80 keV is accepted.

A. Triple-coincidence spectra

Each of the three detectors covers roughly 10% of 4π solid angle, and 9 of the 96 strips were excluded, either because they were dead, because they were partly shaded by the foil holder (Fig. 2) or because of bad resolution or nonlinear energy response. With the remaining strips, however, we can detect all three α particles in coincidence, with an efficiency of 1–4% depending on the kinematics of the breakup.

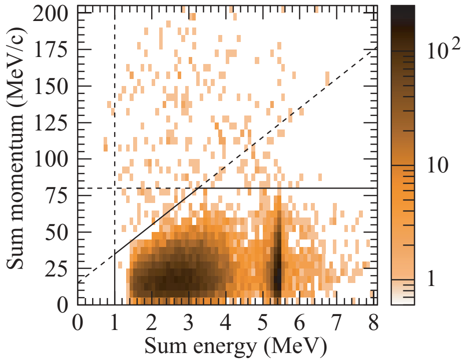

FIG. 3. (Color online) Energy and momentum of potential triple-α events with applied energy-momentum cutoff, ^{12}N-decay data.

The recoil of the nucleus in the β decay depends on the Q value of the decay but has in none of the measured decays an average momentum of more than 5 MeV/c corresponding to a kinetic energy of 1 keV. The laboratory system therefore coincides with the center of mass for the three emitted α particles, for which reason the total momentum of the three α particles can be used to discriminate between triple-coincidence events where all three hits are α particles from a single β-delayed breakup and false coincidences where one or more of the three identified hits is background being either low-energy background or a randomly coincident α particle from a different decay event. In some events (0.7%) more than three hits are identified, resulting in more than one possible coincidence triplet, in which case the triplet with the lowest sum momentum is taken as a potential triple-α coincidence event. As shown in Fig. 3 the triplet is furthermore required to comply with the cutoffs: $E_{\text{sum}} > 1$ MeV and $p_{\text{sum}} < 15\ \text{MeV}/c + 20\, E_{\text{sum}}/c$ and $p_{\text{sum}} < 80\ \text{MeV}/c$. For further details of the analysis, see Ref. [17].

The total triple-coincidence data is shown in Fig. 4 for ^{12}N as well as ^{12}B β-delayed breakup. The plots are scatter plots of the deduced ^{12}C energy versus the three individual α-particle energies as used previously in the analysis of β-delayed 2p decay data in Ref. [29]. In these plots, a single event yields three dots on a horizontal line. When the breakup proceeds through the narrow 92-keV ground state in ^{8}Be, the relation between the energy in ^{12}C and the kinetic energy of the first emitted α particle is:

$$E_{\alpha_1} = \tfrac{2}{3}\left(E_{^{12}\text{C}^*} - E_{^8\text{Be}}\right), \tag{1}$$

which is clearly visible in the data along with the average energy of the two remaining α particles, following a line of slope 6. Both linear relations are indicated in Fig. 4.

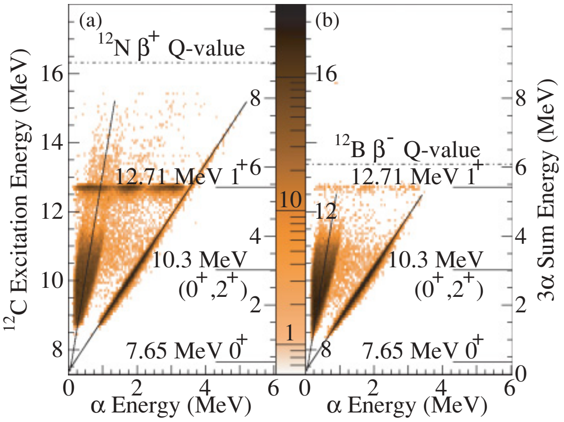

FIG. 4. (Color online) Detected triple-coincidence events; ^{12}N (a) and ^{12}B (b) β-delayed triple-α breakup, respectively. Triple-α sum energy and corresponding ^{12}C excitation energy shown against individual α energy. Coincidence gate applied as indicated in Fig. 3.

In these scatter plots, many of the physical properties of the breakup can be seen at first glance. One aspect is the very pronounced structure around 11 MeV in ^{12}C clearly decaying through the ^{8}Be ground-state channel and in addition to this the 12.7-MeV 1^+ state in ^{12}C evident not only in the ^{12}N data but in the ^{12}B decay as well. The fact that it is a 1^+ state is immediately apparent, because it cannot decay through the ^{8}Be 0^+ ground state (conservation of spin and parity) but must decay through another channel, seen by the completely different sharing of the energy between the three α particles as investigated in detail in Ref. [12]. A third group of breakup events is also seen around 11 MeV in ^{12}C with a broad distribution of α energies around 1.5 MeV. This is the breakup through excited energies in ^{8}Be. Also above the 12.7-MeV 1^+ state some indication of breakup other than through the ^{8}Be(gs) channel is seen. To directly see the improvement in detection efficiency in this experiment for excited energies in ^{8}Be, compare the ^{12}B data to Fig. 3 of Ref. [2]. The 7.654-MeV Hoyle state is not seen in any of the data sets because of low-energy cutoffs.

To distinguish between the ^{8}Be(gs) channel and other breakup events, it is useful to reconstruct the ^{8}Be energy from the kinematics of the breakup. As argued in Refs. [2,17], sensitivity to the experimental resolution is minimized when reconstructing the energy from the relative momentum of the two low-energy α particles (denoted particle 2 and 3):

$$E_{^8\text{Be}} = \frac{{p_{2-3}}^2}{m_\alpha}, \tag{2}$$

following the notation of Ref. [30]. This energy distribution is shown in Figs. 5 and 6 for the ^{12}B and ^{12}N decay data, respectively. All events within 60 keV from the physical energy of the ^{8}Be(gs) are considered ground-state breakup events, whereas events above 200 keV must originate from another mode of breakup. This breakup mode will be investigated in detail in Secs. IV and V.

B. Spectra for breakup through the ^{8}Be ground state

As a first step, however, we will look at breakup through the ^{8}Be ground state and investigate the corresponding β-delayed triple-α spectra. To handle triple-coincidence detection efficiencies correctly, Monte Carlo simulations are necessary. These can be divided into three important steps; first, a physical description of the breakup process; second, the effects of the experimental setup; and, finally, the consequences of the data-analysis procedures as applied to the experimental data.

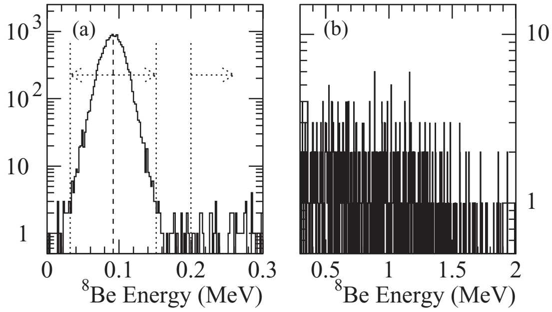

FIG. 5. Energy of the intermediate ^{8}Be nucleus reconstructed from the relative momentum of the two α particles with the lowest energies, shown for ^{12}B-decay data. Energies in the vicinity of the ^{8}Be(0^+) ground-state energy (a) as well as higher reconstructed energies (b) are displayed. In the low-energy region (a) the ^{8}Be ground-state energy [31] (dashed) and cutoffs (dotted) used to distinguish between the ground-state and non-ground-state channels are indicated.

For β-delayed breakup through the ^{8}Be(gs) channel, the physical description of the breakup is straightforward. The breakup is sequential and because the beam of β-decaying nuclei is not polarized and the intermediate ^{8}Be(gs) has spin 0, the two subsequent breakups are isotropic. The kinematics therefore depend on the ^{12}C energy alone. Regarding the experimental setup, the depth distributions of the implanted ions in the carbon foil are simulated using SRIM2003, and with the assumption that the beam profile is Gaussian the beam-spot size is determined to be in the range of 1 to 2.3 mm from comparison of simulated and measured momentum distributions and reconstructed ^{8}Be energy distributions (for details see Ref. [17]). With these assumptions on the spatial characteristics of the decaying nuclei, energy loss corrections are made with SRIM2003 and the detector response is calculated taking into account the uncertainties in setup geometry as well as energy resolution. Simulated data events are then saved as raw data to allow use of exactly the same analysis procedures for simulated data as were used for the physical data, ensuring that low-energy cutoffs, trigger levels, and other constraints are identical in the analysis of physical data and simulated events.

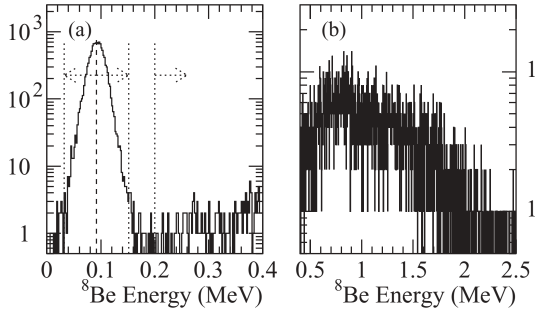

FIG. 6. Reconstructed energy of intermediate ^{8}Be for ^{12}N-decay data, similar to that shown in Fig. 5.

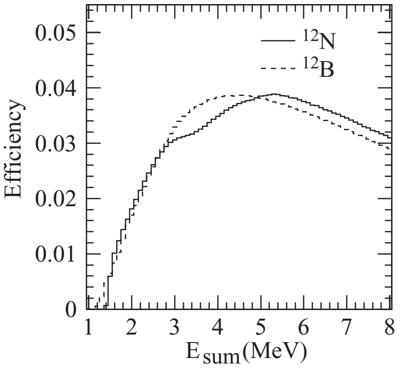

FIG. 7. Simulated triple-coincidence detection efficiencies for ^{12}N and ^{12}B decay data.

In steps of 100 keV, the efficiency is found with 10^7 simulated events yielding a relative statistical uncertainty of less than 1%. The energy-dependent triple-coincidence detection efficiency is shown in Fig. 7 for both ^{12}N and ^{12}B data. The difference seen when comparing ^{12}N and ^{12}B coincidence efficiencies—most pronounced around 3–4 MeV—stems primarily from the different trigger levels used in the two parts of the experiment. For the ^{12}B-decay measurement, trigger levels lower than in the ^{12}N-decay measurement were achieved, giving rise to the deviating detection efficiencies. The effects from the uncertainty in beam-spot size introduce a relative uncertainty of 5–20% in the absolute values of the efficiency, lowest at low energies. The uncertainty in the shape of the efficiency is, however, modest.

The measured β-delayed triple-α spectra for breakup through the ^{8}Be(gs) channel from ^{12}N and ^{12}B β decays are shown in Fig. 8(a), corrected for the different β-decay phase-space factors in the two decays. When furthermore corrected for the simulated detection efficiencies [Fig. 8(b)], the two spectra are consistent in the measured position and shape of the 10.3-MeV strength, indicating a high degree of isospin symmetry in the two decays. The fact that the difference in detection efficiencies so well accounts for the deviation of the ^{12}N with respect to the ^{12}B spectra [Fig. 8(a)] shows that the effect of the trigger levels on the shape of the measured ^{12}C spectrum is well understood.

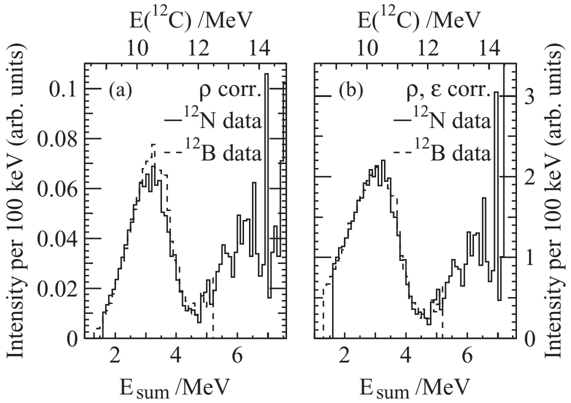

FIG. 8. ^{12}N and ^{12}B spectra corrected for β-decay phase space (a) and furthermore corrected for coincidence detection efficiency (b). Both spectra are for breakup through the ^{8}Be(gs) exclusively.

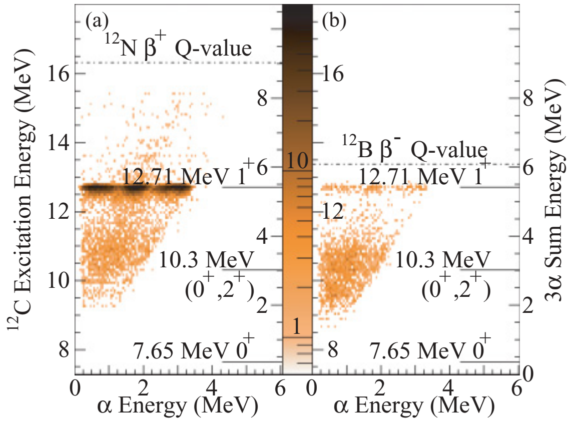

FIG. 9. (Color online) ^{12}N (a) and ^{12}B (b) β-delayed triple-α breakup through the ^{8}Be excited-energy channel. Triple-α sum energies are depicted against individual α energies, and the corresponding ^{12}C energies are shown. Data cuts have been applied as described in the text and illustrated in Figs. 5(a) and 6(a).

IV. BREAKUP DATA FOR ^{12}C STATES

As described in the preceding section, the distinction between breakup through the 92-keV ^{8}Be ground state and other modes of breakup is evident experimentally. We will in the following refer to the latter group of decays as breakup through excited energies in ^{8}Be. The breakup patterns are shown in Fig. 9. The full extent of the broad α group around 11 MeV in ^{12}C is now evident, as opposed to what was seen in the similar spectrum for the full data set (Fig. 4). Note that for the time being these events are not attributed to a specific breakup channel, because we cannot *a priori* claim to know that an excited state resonance of ^{8}Be is playing a role here. The statement "excited energies in ^{8}Be" should therefore be seen as an observational feature—that the reconstructed ^{8}Be energy is significantly higher than the ^{8}Be ground state—rather than a claim about the physical nature of the breakup. The ^{12}C-energy distributions for this breakup channel are also found by projecting the spectra in Fig. 9 onto the sum energy axis and are shown in Fig. 10. The different modes of breakup for this part of the data will be the main focus of the following sections.

A. Phase-space distributions

A thorough analysis of the breakup of the 12.7 MeV 1$^+$ state of ^{12}C has previously been published [12]. This study showed that the breakup could be successfully described as a resonant breakup through the 3 MeV 2$^+$ state of ^{8}Be if the intermediate state was properly described in a fully symmetrized R-matrix model. The direct-breakup model [32], however, could not reproduce the data. Keeping this in mind, we will in Sec. V attempt to describe the measured breakup using an R-matrix description of the intermediate ^{8}Be resonance(s), not only for the 12.7-MeV state but as well for the broad 0$^+$ and 2$^+$ states of ^{12}C. This description combines the effects of the intrinsic symmetry if the ^{12}C state with the restrictions imposed by the intermediate ^{8}Be states in a sequential model of the breakup.

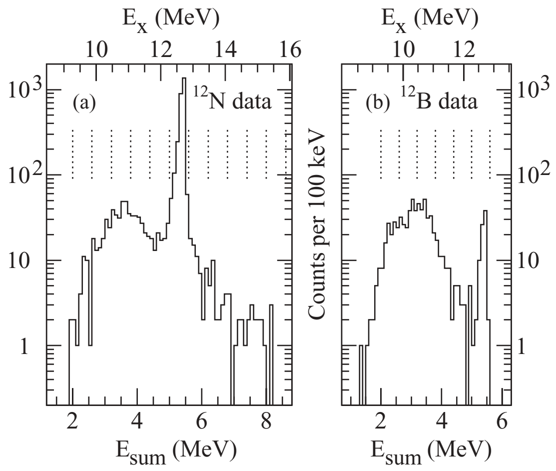

FIG. 10. ^{12}N (a) and ^{12}B (b) β-delayed triple-α breakup through the ^{8}Be excited-energy channel. Binning used for phase-space distributions (Sec. IV A) is indicated (dotted). Measured triple-α sum energy and corresponding ^{12}C excitation energy (E_x) are shown.

The restrictions from the symmetry are imposed on the breakup through the identical nature of the three α particles ($J^\pi = 0^+, T = 0$). For different ^{12}C $T = 0$ states—as relevant for the present analysis—the symmetry is defined by the spin parity of the decaying state. A corresponding analysis of the breakup to the three-pion continuum can be found in Ref. [33]. Because of the different nature of the α particles and pions, three-pion breakup of $T = 3$ states of one parity corresponds to triple-α breakup of $T = 0$ states of the opposite parity. Using this analogy, it is seen from Ref. [33] that the symmetry imposes constraints on the breakup of the 12.7-MeV, $J^\pi = 1^+, T = 0$ state of ^{12}C. For the 12.3- to 12.9-MeV region of Fig. 11, the symmetry therefore excludes the $(x, y) = (0, 0)$ point from the Dalitz plot as well as the two straight edges indicated in the figure. For ^{12}C 0$^+$ and 2$^+$ states, however, no such constraints are imposed on the breakup distributions. The effect of the involved intermediate ^{8}Be state in a sequential description of the breakup is the following: First, the angular correlations as introduced through the spin of the intermediate state and the angular momentum of the first breakup. This is a major effect as will become clear through the following sections. Second, the energy of the intermediate state determines a preferred region of the Dalitz plot, as described in Ref. [13]. The narrower the intermediate state is compared to the total available energy in the triple-α breakup, the stronger is the effect of this on the phase-space distribution. Third, where the states are broad—and because of threshold effects possibly even asymmetric—the shape of the intermediate state comes into play. This is crucial in particular for breakup through the ghost of the ^{8}Be ground state (Sec. V C) and is properly accounted for only when the energy-dependent width of the state is included in the description of the intermediate state, such as is done through for instance R-matrix theory. It is, however, not necessary in the R-matrix description to include interference with higher-lying background levels in ^{8}Be that potentially could change the shape of the 0$^+$ ground

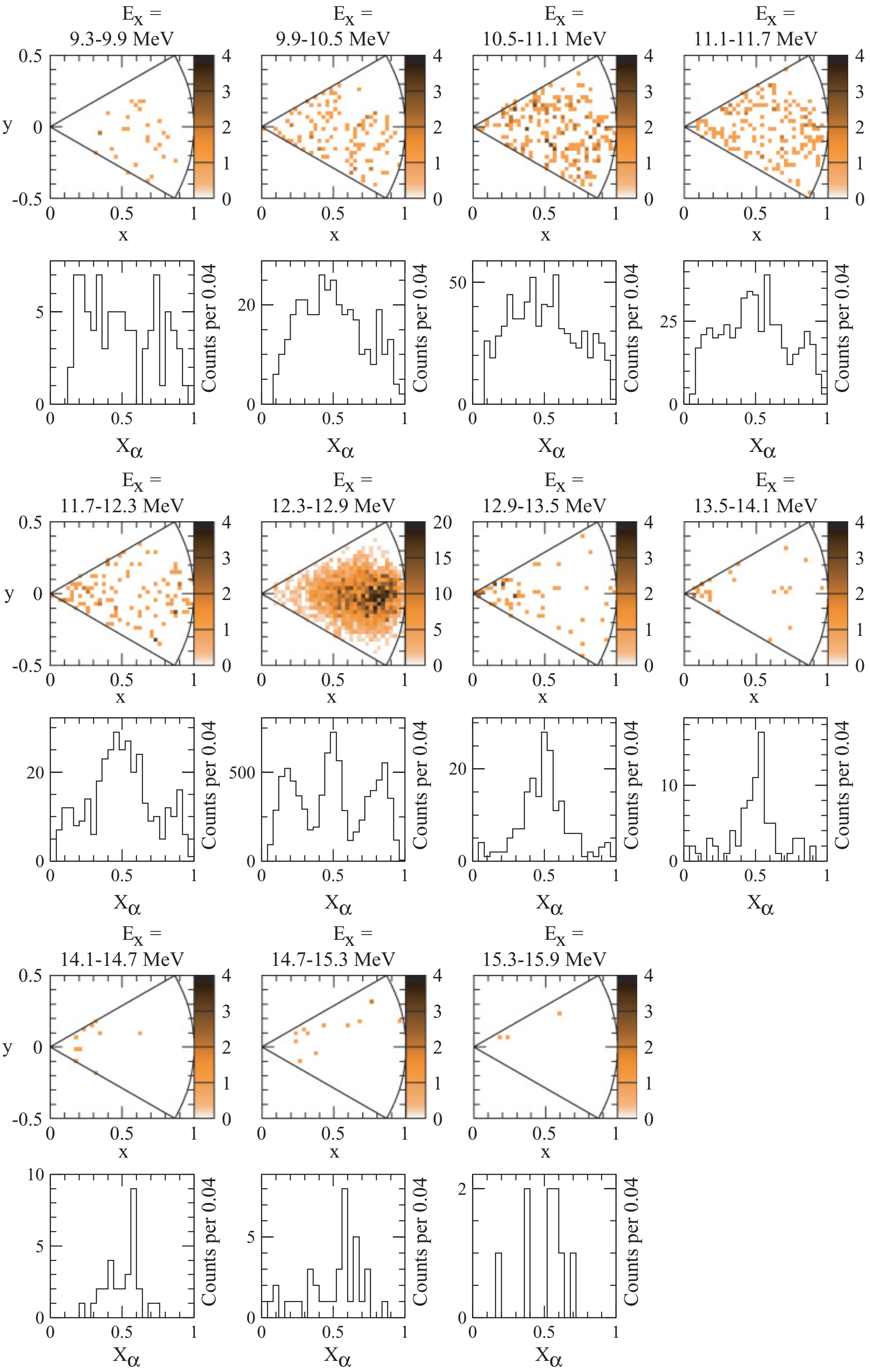

FIG. 11. (Color online) ^{12}N β-delayed triple-α breakup data. Dalitz plots (x, y) defined as described in the text are shown along with individual α energies (X_α) scaled event by event relative to the maximal kinematically allowed α energy. Data is shown for individual ^{12}C excitation energy bins (E_x) as defined in Fig. 10(a).

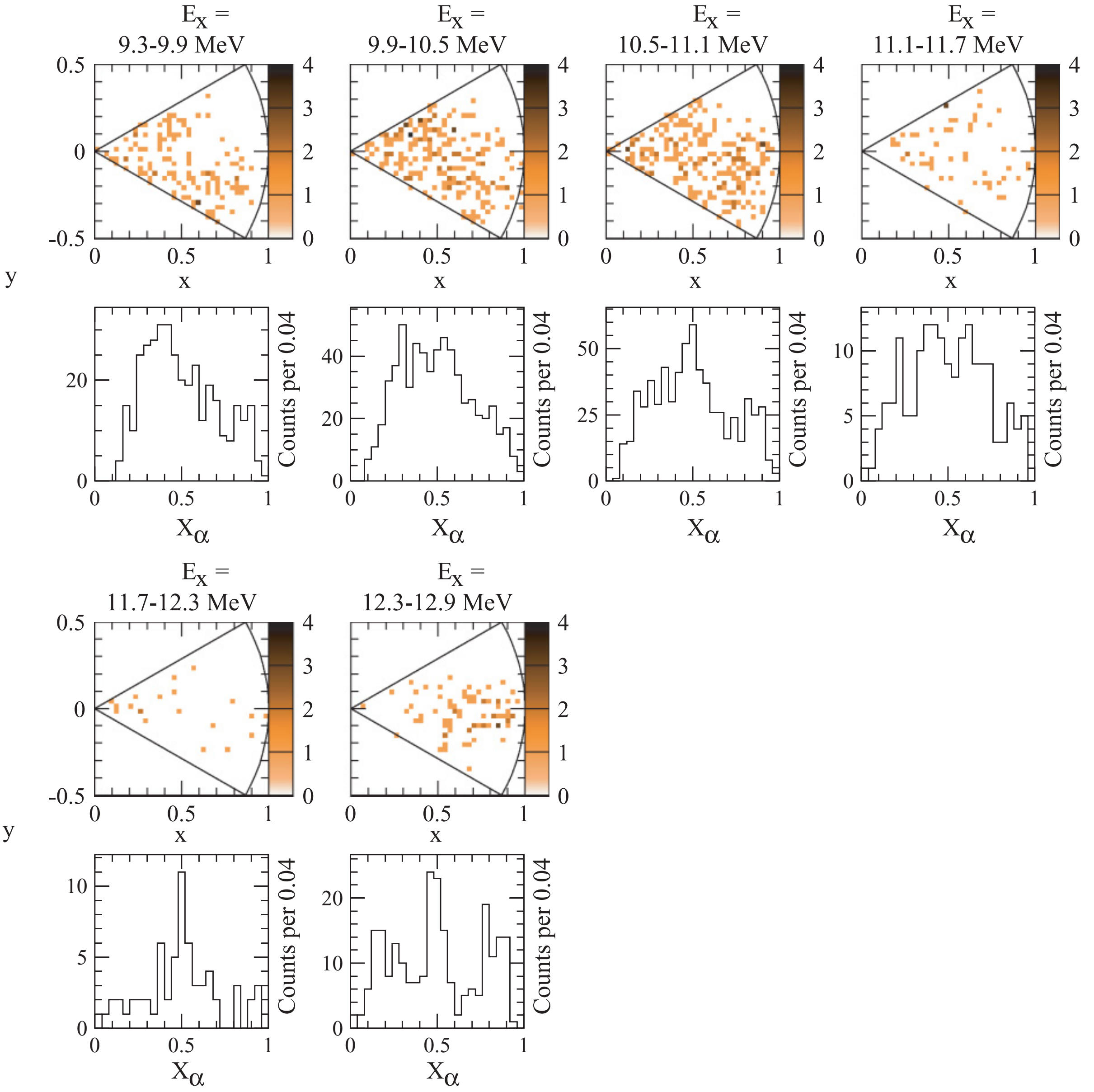

FIG. 12. (Color online) ^{12}B β-delayed triple-α breakup data, defined as in Fig. 11. Data is shown for individual ^{12}C excitation energy bins (E_x) as defined in Fig. 10(b).

state and 2^+ excited state slightly, as the effect of this would be smaller than what the sensitivity of the present experiment justifies.

In the following we will, for different ^{12}C energies, investigate which parts of three-particle phase space dominate the breakup. The data is therefore binned as indicated in Fig. 10. For these bins we plot the individual α energies relative to the maximum kinematically allowed α energy: $X_\alpha = E_\alpha/(\frac{2}{3}E_{\text{sum}})$ as seen in Figs. 11 and 12. An even better way to describe the phase-space distribution is using the two dimensional Dalitz plot [34] where the horizontal and vertical positions in the plot are defined from the α energies as: $x = \sqrt{3}(E_1 - E_3)/E_{\text{sum}}$ and $y = (2E_2 - E_1 - E_3)/E_{\text{sum}}$, respectively. These distributions are also shown in Figs. 11 and 12, where the indicated region is the kinematically allowed region of phase space for breakup into three identical particles [34]. The Dalitz plots in Figs. 11 and 12 are for convenience made with the convention $E_1 > E_2 > E_3$, whereas in the original plot by Dalitz, the convention $E_1 > E_3 > E_2$ was used with the exchange of E_2 and E_3 in the definition of x and y. Data points close to the tip of the region (left) are events with an equal sharing of the energy between the three emitted particles, whereas the points close to the upper right corner correspond to $E_3 \approx 0$ and the lower right corner have $E_1 = \frac{2}{3}E_{\text{sum}}$, the highest possible energy for an individual α particle.

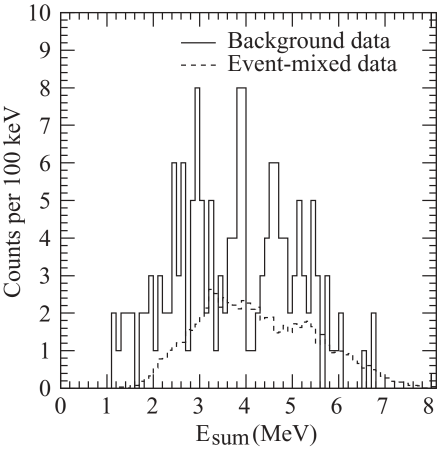

FIG. 13. Estimated background distribution. Shown are the background estimated from energy and momentum cutoffs applied to the data as described in the text (solid line) as well as background estimated using event-mixed data (dashed line). The event-mixed data is scaled by comparison to the data as described in the text.

B. Background estimates

The background intensity and its energy and phase-space distributions have first been estimated from data using the plot of sum-momentum versus sum-energy shown in Fig. 3. The background coincidence events are not expected to comply with momentum conservation by default, and we therefore apply an energy-momentum cutoff similar to that used for the coincidence-event identification but shifted to higher momenta (above 80 MeV/c). With this cutoff, we get the energy distribution shown in Fig. 13 (solid line). The background energy distributions and intensities thus found have been tested using event mixing, where two α particles from one event have been combined with a third α particle taken at random from a different breakup event in the data. The energy spectrum estimated in this way is scaled by comparing the actual data and the event-mixed data just outside the region of sum-momentum and sum-energy accepted as true triple-α coincidences (Fig. 3). This yields a slightly lower background estimate compared to that given above but lends support to the energy distribution as well as the approximate scale. The difference between the two on an absolute scale is not surprising, as the phase space at sum momenta of 80–160 MeV/c is larger than that of the 0–80 MeV/c region, giving rise to a possible overestimation of the background when using the first method. With these spectra in hand and comparing to Fig. 10 we estimate that even for the weak ^{8}Be excited-energy breakup channel, the background is less than 10%, a conclusion which is furthermore confirmed by investigation of the Dalitz plots for the event-mixed data where it is seen that the phase-space distributions of the event-mixed data differ significantly from the distributions of the real data and can therefore at most describe 10% of the data in each sum-energy bin and for most energies significantly less. To properly take into account the effect of background we will in the following quantitative analysis of phase-space distributions (Sec. V D) include a small background contribution to the phase-space distribution as estimated from the event-mixed data.

V. BREAKUP SIMULATIONS AND ANALYSIS

For breakup through excited energies in ^{8}Be as for breakup through the ^{8}Be ground state, there are three components to the Monte Carlo simulations necessary to handle detection efficiencies properly; a physical description of the breakup process, the impact of the limited spatial coverage of the setup, and the effects of cutoffs and thresholds introduced in data taking and analysis. Of these, the latter two are handled as for breakup through the ^{8}Be ground state (Sec. III B). The physical description of the breakup, however, is fundamentally different. Following Refs. [12,35] we describe the breakup in a fully symmetrized R-matrix model with the only difference being the assumed spins and angular momenta as a consequence of our investigation of 0^+ and 2^+ states. All investigated combinations of spins and angular momenta will be discussed in detail in the following sections.

In Fig. 14 an overview of the differences in detection efficiencies as estimated from the breakup simulations are shown. As is seen here, the detection efficiency may—depending on the phase-space distribution and thereby depending on the breakup channel—differ by as much as 25% relative to the average of all breakup channels. The breakup channels shown are for different assumptions on ^{12}C spin [$J(^{12}\text{C})$],

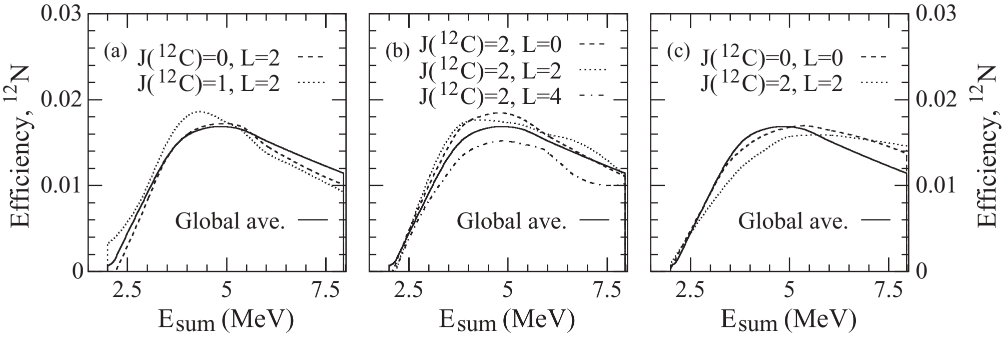

FIG. 14. Triple-α detection efficiencies for different breakup channels. Shown are assumed breakup of ^{12}C states of spin $J(^{12}\text{C})$ with angular momentum L between the first emitted α particle and the remaining ^{8}Be nucleus of spin $J(^{8}\text{Be})$. In (a) and (b), $J(^{8}\text{Be}) = 2$ whereas in (c) $J(^{8}\text{Be}) = 0$ is assumed.

spin of the intermediate ^{8}Be nucleus [$J(^8\mathrm{Be})$], and the relative angular momentum [L] of the ^{8}Be nucleus and the first emitted α particle. Because of the differences in the nature of the individual breakup channels, each investigated channel has been simulated separately. Before investigating the most important breakup of the 0^+ and 2^+ states, we will briefly examine the breakup of the 12.7-MeV 1^+ state of ^{12}C, with which we will validate the following evaluation of the data for 0^+ and 2^+ states of ^{12}C.

A. Breakup of the 12.7-MeV ^{12}C 1^+ state

The physical three-particle phase-space distribution for ^{12}C breakup through the $^8\mathrm{Be}(2^+)$ excited state is found using a fully symmetrized sequential R-matrix description as done in [12,35], where the $J^\pi(^{12}\mathrm{C}) = 1^+$ state emits an $L = 2$ α particle leaving the remaining two in the $J^\pi(^8\mathrm{Be}) = 2^+$ excited state of ^{8}Be. The energy and width of the $^8\mathrm{Be}(2^+)$ state is here taken to be $E_{2+} = 3.03(1)$ MeV and $\Gamma_{2+} = 1.513(15)$ MeV from Ref. [31] with the most significant measurement being that of Ref. [36], whom we also follow in using a channel radius of 4.5 fm. The three-body amplitude is then symmetrized and the resulting phase-space distribution is sampled using the von Neumann sampling method [37]. With the events distributed according to the simulated distribution, the effect of setup geometry, thresholds and data analysis is evaluated for each simulated event, and the event is rejected if a corresponding data event would have been rejected.

In Fig. 15 the result of such a simulation is shown. This simulation is performed for 10^7 physical breakup events yielding in total $1.864(4) \times 10^5$ detected triple-coincidence events corresponding to an efficiency of 1.86%. It is clear that the overall properties are reproduced in the Dalitz plot as well as in the X_α plot. The small negative bias in the y value of the Dalitz plot of about -0.08 compared to the data shown in Fig. 11 (excitation energy 12.3–12.9 MeV) indicates that we should not expect the agreement between data and model to be better than that for the ^{12}C 0^+ and 2^+ state breakups and suggests that a binning coarser than that of the shown Dalitz plots should be used if a bin-by-bin comparison between data and simulation is intended. For further details of the Monte Carlo simulations, see Ref. [17].

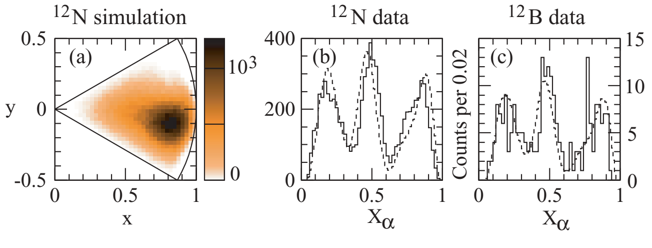

FIG. 15. (Color online) ^{12}C 12.7-MeV 1^+ state breakup through ^{8}Be 2^+ state. R-matrix simulated distribution corresponding to ^{12}N decay data (a). Single-α energy scaled according to maximally allowed α energy with comparison of data (solid) and simulation (dashed) for ^{12}N and ^{12}B data. Simulations are scaled down to reproduce the number of counts in the data sets.

B. The excited $^8\mathrm{Be}(2^+)$ breakup channel

The phase-space distributions for the breakup of ^{12}C 0^+ and 2^+ strengths at any given ^{12}C energy may be sampled in the same way as was done for the $^{12}\mathrm{C}(1^+)$ breakup assuming a breakup through the broad ^{8}Be 2^+ excited state about 3 MeV above the ground state. In the present case, however, more than one angular momentum value is possible if the ^{12}C state in question is a 2^+ state, namely 0, 2, and 4. For breakup of ^{12}C 0^+ states through this ^{8}Be state, only $L = 2$ is allowed. Such simulations for 10^6 simulated events are shown as Dalitz plots in Fig. 16(a). Before making a quantitative comparison of the simulated Dalitz plots and the corresponding experimental data [Fig. 16(c)], we will consider the overall picture from what can be seen by eye. What we should look for in the comparison is not the overall scale of the distributions but in which parts of the Dalitz plots the intensity is located, i.e., which parts of phase space dominate the breakups.

The most pronounced structure seen in the simulations [Fig. 16(a)] is the fact that $L = 2$ simulations are strongly peaked at the origin of the Dalitz plot, whereas the others, especially $L = 0$, show a more uniform distribution. It is therefore clear that neither of the $L = 2$ distributions can dominate the low-energy breakups, whereas $J(^{12}\mathrm{C}) = 2, L = 0$ and $J(^{12}\mathrm{C}) = 2, L = 4$ both resemble the data reasonably well. At higher energies the situation is quite the opposite pointing toward a significant $L = 2$ contribution at these energies. This is consistent with the fact that the angular-momentum barrier is enhanced for $L = 2$ compared to that of an $L = 0$ breakup.

C. Breakup through the ghost of the ^{8}Be ground state

In addition to breakup through the ^{8}Be 2^+ excited state, another channel is in fact available for the breakup; the ^{8}Be ground state is important not only around its resonance 92 keV above threshold but also in the upper tail of the state. The shape of this tail is, as the energy increases, determined by the competition between the increasing denominator in the ground-state line shape and (in the numerator) the rapidly increasing penetration factor for the α-α breakup through the Coulomb barrier [38–41]. This blown-up high-energy tail of the ^{8}Be ground-state distribution is what is known as the ghost of the ^{8}Be ground state. Though physically this is not a separate breakup channel, but rather is a part of the ^{8}Be-ground-state channel [2], experimentally it will mix with the ^{8}Be-2^+ channel and must therefore be considered separately in this context.

With this "excited state" of ^{8}Be an analysis similar to that of the preceding section can be made. The ^{8}Be spin $J(^8\mathrm{Be})$ is now 0, requiring $L = J(^{12}\mathrm{C})$. In addition to the difference in spins and angular momenta, the shape of the 0^+ ghost is very different from that of the 2^+ excited state because of the pronounced threshold effects affecting the ^{8}Be width and its energy dependence. The Dalitz plots for simulations corresponding to a ^{12}C spin $J(^{12}\mathrm{C})$ of 0 and 2 are shown in Fig. 16(b). When comparing these to the measured data [Fig. 16(c)], it is evident that, for the low-energy region, the simulation assuming breakup through the $^8\mathrm{Be}(0^+)$ ghost for $J(^{12}\mathrm{C}) = 0$ and $L = 0$ resembles the data rather well. For the

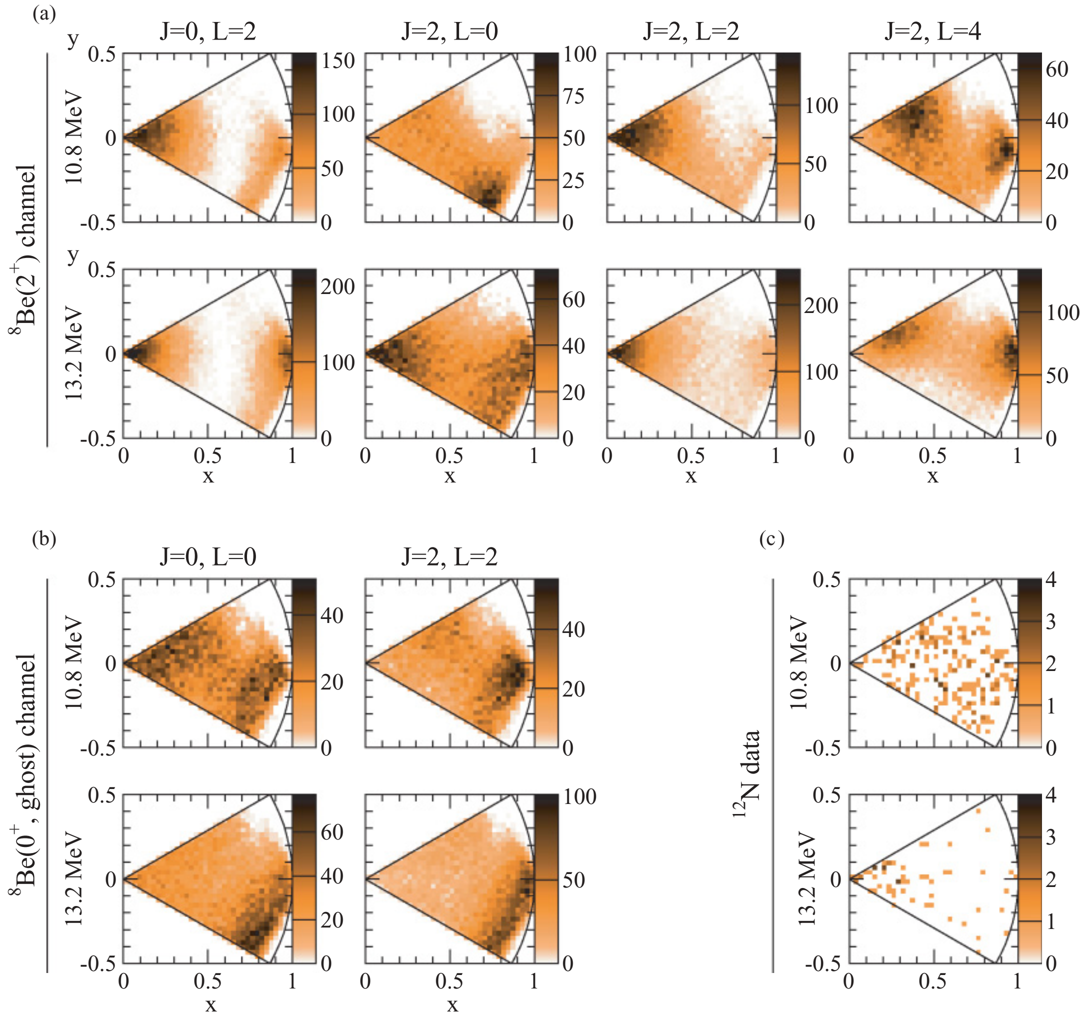

FIG. 16. (Color online) Dalitz plots for ^{12}N phase-space simulations in two different sum-energy bins. Distributions for breakup through ^{8}Be 2^+ state (a) with two different possible spins (J) of the ^{12}C state and all possible angular momenta (L) for the ^{8}Be$(2^+) + \alpha$ intermediate system. Distributions for breakup through the ghost of ^{8}Be(gs) are shown in (b), where the angular momentum (L) equals the ^{12}C state spin (J). In (c) the corresponding distributions as measured in ^{12}N β decay are shown.

higher-energy region, however, it is evident that neither of the two can represent a dominant contribution to the measured breakup, and we must therefore search among the simulations for $J(^8\text{Be}) = 2$.

D. Quantitative analysis of breakup channels

With this understanding of the overall picture, we are ready to proceed to a quantitative analysis of the data. The Dalitz plots shown in the preceding section all have a pixelation of 36 × 36. As noted in Sec. V A, however, the precision of the simulations does not justify such a fine binning of the Dalitz plots. For this reason, and because of the low statistics at most sum energies, the following comparison between data and simulations has been performed for a binning 6 times as coarse, yielding 36 pixels in total. Of these pixels 8 do not overlap with the region of the Dalitz plot obeying $E_1 > E_2 > E_3$ leaving 28 relevant pixels. The simulated distributions have been fitted to the data with one free parameter, a scale factor. In addition to these contributions from the simulated distributions, background components estimated from event mixing have been included, scaled as indicated in Fig. 13. Because of the low statistics we furthermore use maximum-likelihood fitting and indicate the goodness-of-fit using the maximum-likelihood-ratio chi-squared value (χ^2_λ). We subsequently evaluate $\Delta_\chi = \sqrt{2\chi^2_\lambda} - \sqrt{2n'_d - 1}$, where n'_d under normal circumstances should be the number of degrees of freedom of the fits (here $n'_d = 27$ for one parameter fits). This variable will asymptotically follow a Gaussian distribution of width 1 and centroid 0 assuming the fit function is the true generator of the data. A high value of Δ_χ therefore corresponds to a Δ_χ-σ rejection of the fit [42]. With the low statistics that in many cases is about one count per pixel, the expectation value of χ^2_λ deviates, however, from the asymptotic result as noted in Refs. [43–45]. Here the authors give the

TABLE I. Goodness-of-fit $\Delta_\chi = \sqrt{2\chi^2_\lambda} - \sqrt{2n'_d - 1}$ for fits of simulated Dalitz-plot distributions to data. Spins and angular momentum assumptions are given as: $J(^{12}\mathrm{C})$, $J(^{8}\mathrm{Be})$, L. Nine and four ^{12}C excitation energy regions are compared for ^{12}N and ^{12}B-decay data, respectively. Also the value of n'_d for the best fit is given. See text for further discussion of goodness-of-fit.

Nucleus	E_x (MeV)	0,2,2	2,2,0	2,2,2	2,2,4	1,2,2	0,0,0	2,0,2	Counts	n'_d
^{12}N	9.3–9.9	2.2	1.7	1.4	0.8	3.9	0.8	1.7	28	20.2
^{12}N	9.9–10.5	8.6	4.1	6.3	2.0	16.5	1.0	3.2	115	25.5
^{12}N	10.5–11.1	16.5	7.6	13.8	3.0	21.4	1.0	1.5	236	26.2
^{12}N	11.1–11.7	10.0	8.0	9.8	1.3	14.8	−0.7	1.0	163	26.3
^{12}N	12.9–13.5	3.0	4.4	0.2	6.6	14.5	6.7	9.8	61	24.8
^{12}N	13.5–14.1	1.6	2.3	0.7	2.9	6.8	4.0	5.6	26	27.8
^{12}N	14.1–14.7	2.1	1.7	1.1	1.8	3.8	2.8	4.3	10	16.7
^{12}N	14.7–15.3	1.4	0.7	1.1	0.7	3.1	2.4	3.5	12	18.3
^{12}N	15.3–15.9	0.8	0.2	−0.3	0.0	2.1	0.8	1.8	3	10.5
^{12}B	9.3–9.9	9.7	−1.1	5.5	1.7	17.7	−1.2	1.9	123	24.3
^{12}B	9.9–10.5	14.5	3.2	9.6	1.2	24.9	0.3	3.3	209	25.3
^{12}B	10.5–11.1	13.3	7.3	10.9	3.5	21.7	−0.3	3.1	221	26.0
^{12}B	11.1–11.7	3.7	1.8	2.3	−0.4	7.4	0.0	1.4	57	25.2

expected contribution to χ^2_λ per channel as a function of the fitted value in the channel in question $[\chi^2_\lambda(f_{\mathrm{ch}})]$. Though their analysis was performed for a flat distribution, we will use n'_d defined as $\sum_{\mathrm{ch}} \chi^2_\lambda(f_{\mathrm{ch}})$ as an estimate of the expected χ^2_λ value and compare to n'_d as described above. As shown in Refs. [44,45] the variance of $\sqrt{2\chi^2_\lambda}$ will in most cases be identical to or less than the asymptotic limit. By assuming a variance of 1, as used in the following, the resulting significance limits and uncertainty intervals will at worst be conservative. In Table I Δ_χ is shown for the individual ^{12}C energy bins defined in Fig. 10 for energies below as well as above the 12.7-MeV state for the ^{12}N-decay data and below the state for the ^{12}B-decay data.

1. ^{12}*C energies below the 12.7-MeV state*

The overall trends identified by eye are confirmed by the fitting. For the 9.3- to 9.9-MeV energy range, the trigger threshold severely affects our phase-space coverage, as events with an even sharing of the energy are lost. Because this region turns out to be crucial for distinguishing between the breakup for spin- and angular-momentum values [$J(^{12}\mathrm{C})$, $J(^{8}\mathrm{Be})$, L] of [2,2,0] and [0,0,0], the present data are—independent of the statistics—insensitive to this distinction for the energy range of 9.3–9.9 MeV.

For energies from 9.9 to 11.7 MeV it is evident that the simulations for [0,2,2], [2,2,0], [2,2,2], and [1,2,2] poorly represent the data (with rejections at the 3-σ level or more). The fits assuming [2,2,4] and [2,0,2] are in general more reasonable, though the [0,0,0] fits corresponding to the breakup of a $J^\pi = 0^+$ ^{12}C state through the ghost of the $J^\pi = 0^+$ ^{8}Be ground state are consistently superior. The [2,2,4] contribution may furthermore be excluded, as the angular-momentum barrier for $L = 4$ breakup of a $J(^{12}\mathrm{C}) = 2$ state through the $J(^{8}\mathrm{Be}) = 2$ state is much higher than that of the corresponding $L = 2$ breakup. As this breakup is not seen in the data at low energies it is highly unlikely that the $L = 4$ breakup should contribute, and we therefore exclude this channel at low energies. With this we conclude that the 9.9–11.7 MeV excitation energy region in ^{12}C for breakup through the excited energies in ^{8}Be, the data is dominated by ^{12}C 0^+ strength with a possible contribution from ^{12}C 2^+ strength. In either case, the breakup is well described as breakup through the ^{8}Be(0^+,ghost) in a sequential fully symmetrized *R*-matrix model.

We subsequently fit the measured phase-space distributions assuming a combination of 0^+ and 2^+ contributions. In this we find individual fits to ^{12}N and ^{12}B to be consistent and in Table II we give the two contributions for the combined ^{12}N and ^{12}B data corrected for detection efficiency and furthermore give the estimated relative contributions from ^{12}C 2^+ strength in this energy region and breakup channel.

In conclusion we do not find evidence of ^{12}C 2^+ strength in the energy range 9.9–10.5 MeV, whereas for the 10.5- to 11.1-MeV range we see some evidence for it, with the data suggesting a 2^+ contribution of $\frac{N(2^+)}{N(0^+)+N(2^+)} = 0.34(^{+14}_{-13})$ for breakup through the ^{8}Be(0^+,ghost). For the 11.1- to 11.7-MeV energy region though a 2^+ contribution is indicated, only the upper limit is significant. Furthermore, if from the

TABLE II. Total number of estimated breakups corrected for detection efficiencies for ^{12}C 0^+ and 2^+ strength, respectively. All breakups are through the ^{8}Be(0^+,ghost). ^{12}C energies in the range 9.9–11.7 MeV are shown. The ratio of 2^+ to total ^{12}C strength in this breakup channel is given. Results are for combined ^{12}N and ^{12}B data and uncertainties are purely statistical. The uncertainty is denoted as "−lim" in cases where the result within one σ is consistent with zero.

E_x (MeV)	$N(0^+)/10^3$	$N(2^+)/10^3$	$\frac{N(2^+)}{N(0^+)+N(2^+)}$
9.9–10.5	$30(^{+3}_{-5})$	$2(^{+6}_{-\mathrm{lim}})$	$0.07(^{+18}_{-\mathrm{lim}})$
10.5–11.1	$22(^{+4}_{-5})$	$12(^{+5}_{-4})$	$0.34(^{+14}_{-13})$
11.1–11.7	10(2)	3(2)	0.25(17)

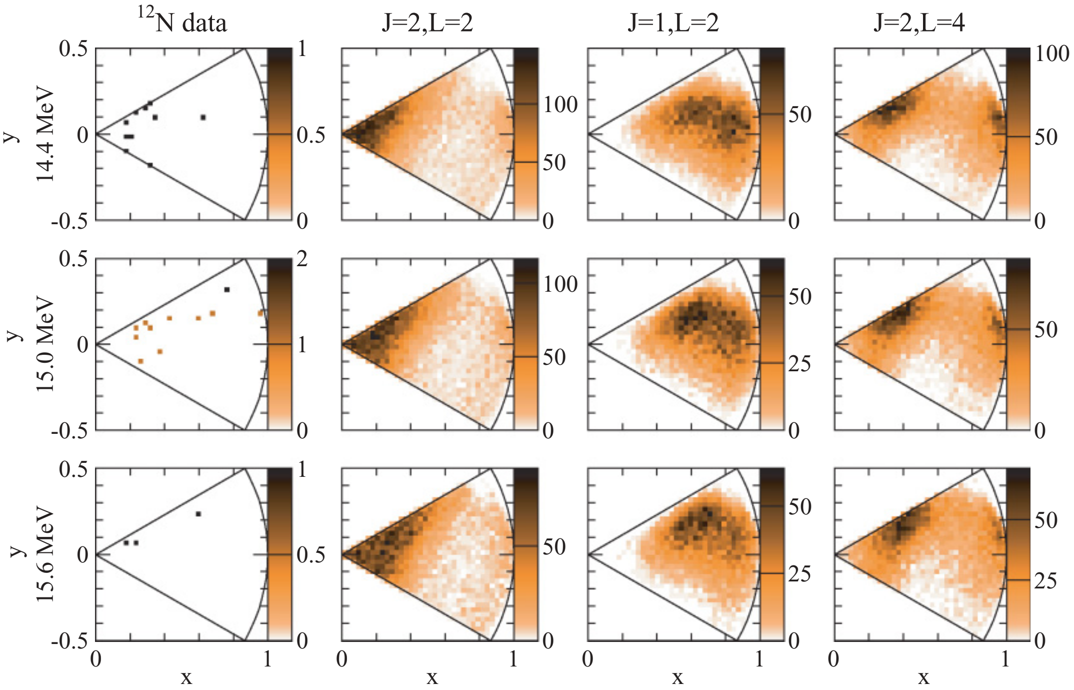

FIG. 17. (Color online) Measured ^{12}N decay data for 14.1- to 14.7-MeV, 14.7- to 15.3-MeV, and 15.3- to 15.9-MeV excitation energy bins (first column) compared to simulations performed at bin centers assuming ^{12}C spin (J) and angular momentum of the $\alpha + {}^{8}$Be pair (L) to be (2,2), (1,2), and (2,4) for the three following columns. All simulations shown assume breakup through the ^{8}Be(2^+) first excited state.

experimental resolution the 12.7-MeV 1^+ state should spill into this energy region, as a very weak branch, this might be mistaken as a ^{12}C(2^+) to ^{8}Be(0^+,ghost) contribution because of the somewhat similar phase-space distributions of the two. This adds a negative systematic uncertainty to the estimated contribution of the 2^+ strength in the 11.1- to 11.7-MeV energy region, emphasizing the interpretation as an upper limit.

2. ^{12}C *energies above the 12.7-MeV state*

For the energy region above the 12.7-MeV state from 12.9 to 14.1 MeV it is evident from Table I that the $[J(^{12}\mathrm{C}), J(^{8}\mathrm{Be}), L] = [2,2,2]$ contribution is superior and must be a dominating breakup channel. For the energy region 14.1–15.3 MeV all three $[2,2,L]$ options for the breakup are possible, whereas the breakup distributions [0,2,2], [1,2,2], [0,0,0], and [2,0,2] are very unlikely as dominant contributions. Based on the fact that the angular-momentum barriers increase with L, it is unlikely that $L = 0$ breakup should contribute significantly at the highest energies while not contributing in the 12.9- to 14.1-MeV energy range, provided the 2^+ strength in the 12.9- to 15.3-MeV energy region is dominated by a single broad state. As this is a reasonable assumption we will in the following discard the [2,2,0] possibility at the highest energies and in further detail investigate the [2,2,2] and [2,2,4] contributions exclusively. For the energy region 15.3–15.9 MeV the statistics does not allow for firm conclusions, though the same trends as seen in the 14.1- to 15.3-MeV energy region seem to be indicated.

In Fig. 17, we show data and simulations for the 14.1- to 14.7-MeV, 14.7- to 15.3-MeV, and 15.3- to 15.9-MeV energy bins. The simulated distributions are shown for the dominating [2,2,2] distributions as well as the possible [2,2,4] distributions. This energy region furthermore covers the 15.1-MeV state in ^{12}C—the isobar analog of the $J^\pi = 1^+, T = 1$ ground states of ^{12}N and ^{12}B—which is known to be fed in the ^{12}N β decay. Additionally, the 15.1-MeV state is known to have a small isospin-forbidden α-decay branch [20,35,46–48]. We therefore for completeness include the [1,2,2] breakup distributions in Fig. 17.

Seeing the [2,2,4] and [1,2,2] breakup as possible contributions in addition to the [2,2,2] breakup in this energy range, we perform separate fits to the measured energy regions for the relevant hypothesis: the [2,2,2] contribution alone ($\mathcal{H}_0$); the [2,2,2] and [2,2,4] combination ($\mathcal{H}_1$); the [2,2,2] and [1,2,2] combination ($\mathcal{H}_2$); and the [2,2,4] contribution alone ($\mathcal{H}_0^*$). In all two component fits we approximate the phase-space distribution by the incoherent sum of the contributions from the two individual channels. The results of this are shown in Table III.

TABLE III. χ^2_λ values for fits of ^{12}N-decay data to [2,2,2] breakup ($\mathcal{H}_0$), [2,2,2] as well as [2,2,4] breakup ($\mathcal{H}_1$), [2,2,2] and [1,2,2] breakup ($\mathcal{H}_2$), and [2,2,4] breakup ($\mathcal{H}_0^*$).

E_x (MeV)	$\chi^2_\lambda(\mathcal{H}_0)$	$\chi^2_\lambda(\mathcal{H}_1)$	$\chi^2_\lambda(\mathcal{H}_2)$	$\chi^2_\lambda(\mathcal{H}_0^*)$
14.1–14.7	22.9	22.9	22.9	27.8
14.7–15.3	24.5	21.9	21.2	22.2
15.3–15.9	8.9	8.9	8.9	10.2

In the fits for $\mathcal{H}_0$ and $\mathcal{H}_0^*$, one fit parameter is varied, whereas for $\mathcal{H}_1$ and $\mathcal{H}_2$ two fit parameters are varied. Furthermore, $\mathcal{H}_0$ is a constrained version of $\mathcal{H}_1$ as well as of $\mathcal{H}_2$ in either case introducing one constraint. Asymptotically, the differences $\chi^2_\lambda(\mathcal{H}_0) - \chi^2_\lambda(\mathcal{H}_1)$ and $\chi^2_\lambda(\mathcal{H}_0) - \chi^2_\lambda(\mathcal{H}_2)$ should therefore follow a $\chi^2(1)$ distribution if $\mathcal{H}_0$ is true [42]. In neither the energy bin around 14.4 MeV nor that around 15.6 MeV do we see a decrease in χ^2_λ by releasing the additional parameter, and we therefore conclude that no evidence for a [2,2,4] or [1,2,2] contribution is seen. However, the possible assumption that all measured events in the 14.1- to 14.7-MeV energy range are from [2,2,4] breakup is rejected with large significance even with the limited statistics available, as the difference $\chi^2_\lambda(\mathcal{H}_0^*) - \chi^2_\lambda(\mathcal{H}_1) = 4.9$ corresponds to a 97% rejection. For the energy range of 14.7–15.3 MeV, the situation is rather different as $\chi^2_\lambda(\mathcal{H}_0) - \chi^2_\lambda(\mathcal{H}_1) = 2.6$ and $\chi^2_\lambda(\mathcal{H}_0) - \chi^2_\lambda(\mathcal{H}_2) = 3.3$ correspond to rejection probabilities for $\mathcal{H}_0$ of 89% and 93% when comparing to $\mathcal{H}_1$ and $\mathcal{H}_2$, respectively. We therefore conclude that some contribution other than [2,2,2] is likely in this energy region. The fit of the 14.7- to 15.3-MeV region assuming a combination of [2,2,2] and [1,2,2] breakup indicates an efficiency-corrected contribution of [1,2,2] breakup corresponding to $4(^{+3}_{-2}) \times 10^2$ β-delayed triple-α decays through the 15.1 MeV 1^+ state, with the remaining $6(^{+3}_{-2}) \times 10^2$ decays arising from the 2^+ breakup. With $1.41(7) \times 10^5$ decays through the 12.7-MeV state (corrected for detection efficiency) we may estimate the relative branching ratio for the 15.1-MeV state, yielding $\mathrm{BR}_\beta^{15.1} \frac{\Gamma_\alpha^{15.1}}{\Gamma^{15.1}} = 2.5(2) \times 10^{-3} \mathrm{BR}_\beta^{12.7}$. This exceeds that found through the previously mentioned implantation experiment [18] by a factor of 10. We therefore conclude it to be unlikely that the breakup data in Fig. 17 should contain a significant contribution from the decay of the 15.1-MeV 1^+ state. For further discussion of absolute branching ratios as deduced from the present experiment, see the detailed analysis in Refs. [18,19]

With breakup of the 15.1-MeV state excluded as a significant contribution to the measured spectra, the only realistic alternative is a combination of [2,2,2] and [2,2,4] breakup. We therefore in Table IV show the [2,2,2] and [2,2,4] contributions as estimated from the fits to the measured phase-space distributions. For the 14.7- to 15.3-MeV region this yields a sharing between the breakup channels of $\frac{N_{224}}{N_{222}+N_{224}} = 0.8(^{+\mathrm{lim}}_{4})$ taking into account the correlation between N_{222} and N_{224}.

TABLE IV. Total number of estimated breakups corrected for detection efficiencies for ^{12}C 2^+ strength decaying through the ^{8}Be(2^+) state with $L = 2$ and $L = 4$, respectively. ^{12}C energies in the range 14.1–15.9 MeV are shown. Results are for ^{12}N data only and uncertainties shown are statistical.

E_x (MeV)	$N_{222}/10^3$	$N_{224}/10^3$
14.1–14.7	0.5(2)	$0.0(^{+2}_{-\mathrm{lim}})$
14.7–15.3	$0.2(^{+5}_{-\mathrm{lim}})$	$0.8(^{+6}_{-5})$
15.3–15.9	0.2(2)	$0.0(^{+2}_{-\mathrm{lim}})$

In conclusion we see that the energy region above the 12.7-MeV state is dominated by a broad 2^+ strength in ^{12}C with a significant breakup via the ^{8}Be 2^+ first excited state.

VI. DISCUSSION

Summarizing the two main breakup channels—breakup through the ^{8}Be ground state and excited energies, respectively—we show the total number of breakups in Table V corrected for triple-α-detection efficiencies. For efficiency corrections of ^{8}Be(ex)-channel data, the average efficiencies as shown in Fig. 14 have been used for ^{12}N-decay data and similarly for ^{12}B data. From this table it is clear that the relative contribution of the ^{8}Be(ex) channel varies strongly with energy even when disregarding the obvious effect of the 12.7-MeV 1^+ state.

At the lowest energies below 10-MeV excitation energy, the contribution through excited energies of ^{8}Be is less than 10%, whereas at energies only 1–2 MeV above this, we see 20–30% contribution from this channel. As argued in the preceding sections, all breakups in this region could successfully be described as proceeding through the ^{8}Be(0^+) state when including the contribution of the ghost of the state. The different energy dependence of the two breakup channels should therefore be attributed solely to the different energy dependence of the involved breakup penetrabilities. As the total width of the 0_3^+ state present in the 10.3-MeV region includes both breakup channels, a detailed description of the shape of the 10.3-MeV 0^+ strength should include not only the interference between the Hoyle-state ghost and the 0_3^+ state as previously discussed [2] but should also include the effect on the energy dependent partial width for breakup through the ^{8}Be ground-state ghost. This, naturally, is true for the description of the Hoyle-state ghost as well as that of the 10.3-MeV state, and

TABLE V. Efficiency-corrected breakup contributions from the ^{8}Be(gs) and ^{8}Be(ex) channels for ^{12}N as well as ^{12}B decay. Uncertainties are combined statistical and systematic.

E_x/MeV	$N_{^{12}\mathrm{N}}/10^3$ ^{8}Be(gs)	$N_{^{12}\mathrm{N}}/10^3$ ^{8}Be(ex)	$N_{^{12}\mathrm{B}}/10^3$ ^{8}Be(gs)	$N_{^{12}\mathrm{B}}/10^3$ ^{8}Be(ex)
8.1–8.7	–	–	$162(^{+32}_{-30})$	–
8.7–9.3	$148(^{+15}_{-10})$	–	$278(^{+27}_{-19})$	$17(^{+6}_{-6})$
9.3–9.9	$148(^{+14}_{-10})$	$9.1(^{+21}_{-20})$	$246(^{+23}_{-16})$	$22.0(^{+29}_{-25})$
9.9–10.5	$128(^{+13}_{-9})$	$14.2(^{+20}_{-17})$	$154(^{+16}_{-11})$	$19.1(^{+24}_{-19})$
10.5–11.1	$72(^{+9}_{-6})$	$18.0(^{+25}_{-18})$	$58(^{+7}_{-5})$	$15.1(^{+21}_{-15})$
11.1–11.7	$15.9(^{+22}_{-14})$	$10.4(^{+16}_{-11})$	$7.6(^{+11}_{-7})$	$3.4(^{+6}_{-5})$
11.7–12.3	$4.1(^{+7}_{-5})$	$6.7(^{+13}_{-8})$	$0.73(^{+18}_{-15})$	$1.2(^{+3}_{-3})$
12.3–12.9	$4.1(^{+8}_{-5})$	$165(^{+30}_{-17})$	$0.13(^{+6}_{-6})$	$4.6(^{+10}_{-7})$
12.9–13.5	$2.8(^{+6}_{-4})$	$3.9(^{+9}_{-7})$	–	–
13.5–14.1	$1.4(^{+4}_{-3})$	$1.8(^{+5}_{-4})$	–	–
14.1–14.7	$0.52(^{+17}_{-14})$	$0.76(^{+29}_{-26})$	–	–
14.7–15.3	$0.12(^{+7}_{-6})$	$1.00(^{+37}_{-32})$	–	–
15.3–15.9	–	$0.27(^{+17}_{-16})$	–	–

interestingly we should therefore expect the ^{8}Be ground-state ghost to affect the shape of the ^{12}C Hoyle-state ghost.

At energies above the 12.7-MeV state as probed in the ^{12}N β decay [Table V], the ^{8}Be(ex) channel is a dominant contribution. It will therefore dominate also the energy dependence of the width of the involved state(s)—in particular that of the ^{12}C(2^+) strength found in this region. That is, for a detailed understanding of the shape of the 2^+ strength contributions to the measured breakup in this energy region, not only must the interference with a possible 2^+ state in the 10- to 11-MeV region be considered but also the inclusion of the energy-dependent partial widths to all channels is essential.

As the analysis of spectrum shapes therefore requires the combination of the present data—for a full description of reaction channels—with decay data including decay through the Hoyle state, such an analysis lies outside the scope of the present article. For future reference, the raw data and average detection efficiencies for both reaction channels are instead made available [49].

VII. CONCLUSIONS

With this we conclude that, at the level of detail allowed by present measurement, the observed breakup data are well described by the applied sequential model. Due to the broad nature of the ^{8}Be(2^+) exited state, we expect only subtle differences between sequential breakup through this state and direct breakup. Only an experiment with significantly higher statistics would therefore be sensitive to the possibility of breakup of a more direct nature.

For the high-energy region (above the ^{12}C 1^+ state at 12.7 MeV) we conclude that the observed breakup is dominated by the breakup of a ^{12}C 2^+ state through the 3-MeV 2^+ state of ^{8}Be as well as through the ^{8}Be ground state. In addition to this we may conclude that at these energies the breakup through the ^{8}Be 2^+ excited state is well described by a d-wave ($L = 2$) component in the intermediate $^{8}\mathrm{Be} + \alpha$ system, though for the highest energies (above 14.7 MeV) some indication of a g-wave component ($L = 4$) is seen.

At energies below the ^{12}C 12.7-MeV state no indication of decay through the ^{8}Be 2^+ excited state is seen and most decays proceed through the ^{8}Be 0^+ ground state. We do, however, see a significant contribution from breakup through the ghost of the ^{8}Be ground state with distinct phase-space distributions. The ^{12}C strength contributing to the breakup through the ^{8}Be(0^+,ghost) and thereby to the breakup as a whole is furthermore shown to be almost exclusively 0^+ strength, in line with previous measurements. For the energy range of 10.5–11.1 MeV, however, the data are consistent with a ^{12}C(2^+) contribution to the β-delayed breakup. This energy range is higher than that suggested by (α, α') scattering experiments [3,22] and is more in line with the 11.16-MeV state previously speculated to be of possible 2^+ character [13,50].

These conclusions are consistent with those from the analysis of the breakup through the 92-keV ^{8}Be ground-state channel presented in Ref. [2]. The resulting spin assignments from the analysis of breakup through the ^{8}Be ground-state channel and the ^{8}Be non-ground-state channels can thereby be seen as independent tests of the ^{12}C state properties, first, because the data are statistically independent and, second, because the previous analysis was built on an understanding of the shape of the ^{12}C spectrum, whereas the analysis presented here focuses on the correlations between the three emitted α particles.

ACKNOWLEDGMENTS

This work was supported by the Academy of Finland under the Finnish Center of Excellence Programme 2000–2005 (Project No. 44875, Nuclear and Condensed Matter Physics Programme at JYFL); by the European Union Fifth Framework Programme “Improving Human Potential—Access to Research Infrastructure,” Contract No. HPRI-CT-1999-00044; by the Spanish CICYT Agency under project number FPA2007-62170 and the MICINN Consolider project CSD2007-00042; and by the EU-RI3 (Integrated Infrastructure Initiative) under Contract No. 506065.

---

[1] M. Freer, Rep. Prog. Phys. **70**, 2149 (2007).

[2] C. Aa. Diget, F. C. Barker, M. J. G. Borge, J. Cederkäll, V. N. Fedosseev, L. M. Fraile, B. R. Fulton, H. O. U. Fynbo, H. B. Jeppesen, B. Jonson, U. Köster, M. Meister, T. Nilsson, G. Nyman, Y. Prezado, K. Riisager, S. Rinta-Antila, O. Tengblad, M. Turrion, K. Wilhelmsen, and J. Äystö, Nucl. Phys. **A760**, 3 (2005).

[3] M. Itoh, Mod. Phys. Lett. A **21**, 2359 (2006).

[4] A. Tamii, T. Adachi, K. Fujita, K. Hatanaka, H. Hashimoto, M. Itoh, H. Matsubara, K. Nakanishi, Y. Sakemi, Y. Shimbara, Y. Shimizu, Y. Tameshige, M. Yosoi, Y. Fujita, H. Sakaguchi, J. Zenihiro, T. Kawabata, Y. Sasamoto, M. Dozono, J. Carter, H. Fujita, B. Rubio, and A. Perez, Mod. Phys. Lett. A **21**, 2367 (2006).

[5] Y. Kanada-En'yo, Prog. Theor. Phys. **117**, 655 (2007).

[6] R. Álvarez-Rodríguez, E. Garrido, A. S. Jensen, D. V. Fedorov, and H. O. U. Fynbo, Eur. Phys. J. A **31**, 303 (2007).

[7] C. Angulo, M. Arnould, M. Rayet, P. Descouvemont, D. Baye, C. Leclercq-Willain, A. Coc, S. Barhoumi, P. Aguer, C. Rolfs, R. Kunz, J. W. Hammer, A. Mayer, T. Paradellis, S. Kossionides, C. Chronidou, K. Spyrou, S. Degl'Innocenti, G. Fiorentini, B. Ricci, S. Zavatarelli, C. Providencia, H. Wolters, J. Soares, C. Grama, J. Rahighi, A. Shotter, and M. Lamehi Rachti, Nucl. Phys. **A656**, 3 (1999).

[8] H. O. U. Fynbo, C. Aa. Diget, U. C. Bergmann, M. J. G. Borge, J. Cederkäll, P. Dendooven, L. M. Fraile, S. Franchoo, V. N. Fedosseev, B. R. Fulton, W. Huang, J. Huikari, H. B. Jeppesen, A. S. Jokinen, P. Jones, B. Jonson, U. Köster, K. Langanke, M. Meister, T. Nilsson, G. Nyman, Y. Prezado, K. Riisager, S. Rinta-Antila, O. Tengblad, M. Turrion, Y. Wang, L. Weissman, K. Wilhelmsen, J. Äystö, and The ISOLDE Collaboration, Nature **433**, 136 (2005).

[9] C. Aa. Diget, M. J. G. Borge, R. Boutami, P. Dendooven, T. Eronen, S. P. Fox, B. R. Fulton, H. O. U. Fynbo, H. B.

Jeppesen, A. Jokinen, B. Jonson, A. Kankainen, I. Moore, A. Nieminen, S. G. Pedersen, H. Penttilä, V. F. E. Pucknell, K. Riisager, S. Rinta-Antila, O. Tengblad, Y. Wang, K. Wilhelmsen, and J. Áystö, in *Proceedings of the International Symposium on Nuclear Astrophysics—Nuclei in the Cosmos—IX, CERN, 2006* (Proceedings of Science, SISSA, Trieste, 2006), p. 25.

[10] L. R. Buchmann and C. A. Barnes, Nucl. Phys. **A777**, 254 (2006).

[11] B. Blank and M. J. G. Borge, Prog. Part. Nucl. Phys. **60**, 403 (2008).

[12] H. O. U. Fynbo, Y. Prezado, U. C. Bergmann, M. J. G. Borge, P. Dendooven, W. X. Huang, J. Huikari, H. Jeppesen, P. Jones, B. Jonson, M. Meister, G. Nyman, K. Riisager, O. Tengblad, I. S. Vogelius, Y. Wang, L. Weissman, K. Wilhelmsen Rolander, and J. Äystö, Phys. Rev. Lett. **91**, 082502 (2003).

[13] M. Freer, I. Boztosun, C. A. Bremner, S. P. G. Chappell, R. L. Cowin, G. K. Dillon, B. R. Fulton, B. J. Greenhalgh, T. Munoz-Britton, M. P. Nicoli, W. D. M. Rae, S. M. Singer, N. Sparks, D. L. Watson, and D. C. Weisser, Phys. Rev. C **76**, 034320 (2007).

[14] R. Álvarez-Rodríguez, A. S. Jensen, E. Garrido, D. V. Fedorov, and H. O. U. Fynbo, Phys. Rev. C **77**, 064305 (2008).

[15] R. Álvarez-Rodríguez, A. S. Jensen, D. V. Fedorov, H. O. U. Fynbo, and E. Garrido, Phys. Rev. Lett. **99**, 072503 (2007).

[16] H. O. U. Fynbo, U. C. Bergmann, M. J. G. Borge, P. Dendooven, C. Aa. Diget, W. Huang, J. Huikari, H. Jeppesen, B. Jonson, P. Jones, M. Meister, G. Nyman, Y. Prezado, K. Riisager, I. Storgaard Vogelius, O. Tengblad, Y. Wang, L. Weissman, K. Wilhelmsen Rolander, and J. Äystö, Nucl. Phys. **A718**, 541c (2003).

[17] C. Aa. Diget, Ph.D. thesis, University of Aarhus, Denmark, 2006, http://www.phys.au.dk/main/publications/PhD/Christian_Aa_Diget.pdf.

[18] S. Hyldegaard, C.Forssén, C. Aa. Diget, M. Alcorta, F. C. Barker, B. Bastin, M. J. G. Borge, R. Boutami, S. Brandenburg, J. Bücher, P. Dendooven, P. Van Duppen, T. Eronen, S. Fox, B. R. Fulton, H. O. U. Fynbo, J. Huikari, M. Huyse, H. B. Jeppesen, A. Jokinen, B. Jonson, K. Jungmann, A. Kankainen, O. Kirsebom, M. Madurga, I. Moore, P. Navrátil, T. Nilsson, G. Nyman, G. J. G. Onderwater, H. Penttilä, K. Peräjärvi, R. Raabe, K. Riisager, S. Rinta-Antila, A. Rogachevskiy, A. Saastamoinen, M. Sohani, O. Tengblad, E. Traykov, J. P. Vary, Y. Wang, K. Wilhelmsen, H. W. Wilschut, and J. Äystö, Phys. Lett. **B678**, 459 (2009).

[19] S. Hyldegaard, C. Aa. Diget, M. J. G. Borge, R. Boutami, P. Dendooven, T. Eronen, S. P. Fox, L. M. Fraile, B. R. Fulton, H. O. U. Fynbo, J. Huikari, H. B. Jeppesen, A. S. Jokinen, B. Jonson, A. Kankainen, I. Moore, G. Nyman, H. Penttilä, K. Peräjärvi, K. Riisager, S. Rinta-Antila, O. Tengblad, Y. Wang, K. Wilhelmsen, and J. Äystö *et al.* (2009) (in press).

[20] F. Ajzenberg-Selove, Nucl. Phys. **A506**, 1 (1990).

[21] Bency John, Y. Tokimoto, Y.-W. Lui, H. L. Clark, X. Chen, and D. H. Youngblood, Phys. Rev. C **68**, 014305 (2003).

[22] M. Itoh, H. Akimune, M. Fujiwara, U. Garg, H. Hashimoto, T. Kawabata, K. Kawase, S. Kishi, T. Murakami, K. Nakanishi, Y. Nakatsugawa, B. K. Nayak, S. Okumura, H. Sakaguchi, H. Takeda, S. Terashima, M. Uchida, Y. Yasuda, M. Yosoi, and J. Zenihiro, Nucl. Phys. **A738**, 268 (2004).

[23] J. Äystö, Nucl. Phys. **A693**, 477 (2001).

[24] O. Tengblad, U. C. Bergmann, L. M. Fraile, H. O. U. Fynbo, and S. Walsh, Nucl. Instrum. Methods A **525**, 458 (2004).

[25] R. B. Firestone and V. S. Shirley, *Table of Isotopes*, 8th ed. (John Wiley & Sons, New York, 1996).

[26] E. T. H. Clifford, E. Hagberg, J. C. Hardy, H. Schmeing, R. E. Azuma, H. C. Evans, V. T. Koslowsky, U. J. Schrewe, K. S. Sharma, and I. S. Towner, Nucl. Phys. **A493**, 293 (1989).

[27] U. C. Bergmann, H. O. U. Fynbo, and O. Tengblad, Nucl. Instrum. Methods A **515**, 657 (2003).

[28] J. F. Ziegler, J. P. Biersack, and U. Littmark, *The Stopping and Range of Ions in Solids* (Pergamon Press, New York, 2003).

[29] H. O. U. Fynbo, M. J. G. Borge, L. Axelsson, J. Äystö, U. C. Bergmann, L. M. Fraile, A. Honkanen, P. Hornshøj, Y. Jading, A. Jokinen, B. Jonson, I. Martel, I. Mukha, T. Nilsson, G. Nyman, M. Oinonen, I. Piqueras, K. Riisager, T. Siiskonen, M. H. Smedberg, O. Tengblad, J. Thaysen, F. Wenander, and The ISOLDE Collaboration, Nucl. Phys. **A677**, 38 (2000).

[30] G. G. Ohlsen, Nucl. Instrum. Methods **37**, 240 (1965).

[31] D. R. Tilley, J. H. Kelley, J. L. Godwin, D. J. Millener, J. Purcell, C. G. Sheu, and H. R. Weller, Nucl. Phys. **A745**, 155 (2004).

[32] A. A. Korsheninnikov, Sov. J. Nucl. Phys. **52**, 827 (1990).

[33] C. Zemach, Phys. Rev. **133**, B1201 (1964).

[34] R. Dalitz, Phil. Mag. **44**, 1068 (1953).

[35] D. P. Balamuth, R. W. Zurmühle, and S. L. Tabor, Phys. Rev. C **10**, 975 (1974).

[36] M. Bhattacharya and E. G. Adelberger, Phys. Rev. C **65**, 055502 (2002).

[37] J. von Neumann, Nat. Bur. Stand. (U. S.), Appl. Math. Ser. **12**, 36 (1951).

[38] F. C. Barker, H. J. Hay, and P. B. Treacy, Aust. J. Phys. **21**, 239 (1967).

[39] F. C. Barker and P. B. Treacy, Nucl. Phys. **38**, 33 (1962).

[40] F. D. Becchetti, C. A. Fields, R. S. Raymond, H. C. Bhang, and D. Overway, Phys. Rev. C **24**, 2401 (1981).

[41] A. Szczurek, K. Bodek, L. Jarczyk, B. Kamys, J. Krug, W. Lübcke, H. Rühl, M. Steinke, M. Stephan, D. Kamke, and A. Strzałkowski, Nucl. Phys. **A531**, 77 (1991).

[42] W. T. Eadie, D. Drijard, F. E. James, M. Roos, and B. Sadoulet, *Statistical Methods in Experimental Physics* (North-Holland, Amsterdam, 1971).

[43] T. Hauschild and M. Jentschel, Nucl. Instrum. Methods A **457**, 384 (2001).

[44] U. C. Bergmann and K. Riisager, Nucl. Phys. **A701**, 213c (2002).

[45] K. J. Mighell, Astrophys. J. **518**, 380 (1999).

[46] D. E. Alburger and D. H. Wilkinson, Phys. Rev. **153**, 1061 (1967).

[47] D. E. Alburger and D. H. Wilkinson, Phys. Rev. C **5**, 384 (1972).

[48] E. G. Adelberger, R. E. Marrs, K. A. Snover, and J. E. Bussoletti, Phys. Rev. C **15**, 484 (1977).

[49] See EPAPS Document No. E-PRVCAN-80-001909 for raw data and detection efficiencies. For more information on EPAPS, see http://www.aip.org/pubservs/epaps.html.

[50] G. M. Reynolds, D. E. Rundquist, and R. M. Poichar, Phys. Rev. C **3**, 442 (1971).